CONF-960928--1

The Oxidation Behavior of Iron Aluminides at 1300°C

M. J. Bennett,* J. H. DeVan, and P. F. Tortorelli
Metals and Ceramics Division
Oak Ridge National Laboratory
P.O. Box 2008
Oak Ridge, Tennessee 37831-6156

ABSTRACT

The oxidation behavior of iron-aluminum alloys, in air and oxygen, at 1300°C has been studied with particular emphasis on the time to loss of protectiveness with onset of breakaway attack. The role of alloy aluminum content between 8.4 and 15.8 w/o and of the addition of a reactive element, zirconium, up to 0.2 w/o, were examined. The periods over which the oxide scales remained protective were quantitatively correlated with aluminum depletion in the alloy substrate. Times to the onset of breakaway for Fe_3Al-Zr have been compared with those for commercial ODS FeCrAl alloys containing Y_2O_3 (MA 956, PM 2000, ODM 751). Characterization of the oxidation of the Fe_3Al-Zr alloys was undertaken using a range of surface analytical procedures, including x-ray diffraction, optical microscopy, scanning and scanning transmission electron microscopy with associated energy dispersive x-ray spectroscopy, and electron microprobe analysis.

INTRODUCTION

Numerous emerging industrial applications require the operation of FeCrAlRE (where RE is a reactive element) structural components at ultrahigh temperatures (that is, ≥1100°C) for assured service lifetimes of at least 20,000 h. Currently available commercial alloys include the Fecralloy† (FeCrAlY) family of wrought steels and the Y_2O_3 oxide-dispersion-strengthened (ODS) alloys MA 956, PM 2000, and ODM 751, which contain up to 20 w/o Cr and 5.5 w/o Al. The corrosion resistance of these alloys is governed by the formation and maintenance of alumina scales. Component service lifetimes of the ODS alloys are determined ultimately by the chemical failure of the protective alumina scale resulting in the onset of non-protective oxidation with the rapid formation of chromium and iron oxides.[1-3] The three factors controlling chemical failure are first, the available aluminum reservoir (that is, a combination of the Al concentration in the alloy and the component thickness), the rate of aluminum consumption (arising from the scale growth rate and exacerbated by spallation),

*Materials Research Consultant, "Three Chimneys," South Moreton, Oxon OX11 9AH, United Kingdom.

†Fecralloy is a registered trademark of the UKAEA.

and, finally, the critical alloy aluminum concentration needed to sustain the formation and integrity of the protective scale.

An alternative iron-based, alumina forming alloy system, currently under development, is based on the iron aluminides,[4] which offer the prospect of a greater Al reservoir with elemental concentrations up to ~16 w/o for Fe_3Al and even higher for the FeAl type of alloys. Some of these alloys have been shown to have outstanding corrosion resistance in sulfidizing environments at 800°C and in air and oxygen at ≤1100°C.[5,6] The purpose of the present study was to explore (1) the boundaries of potential industrial applicability of the iron-aluminum alloys in air up to 1300°C by determining the times to breakdown of their protective oxidation behavior and (2) the role of alloy aluminum content between 8.4 and 15.8 w/o. Several of these alloys contain zirconium as a reactive element addition and the effect of varying its concentration up to 0.2 w/o was also examined.

EXPERIMENTAL PROCEDURES

Four iron-aluminum alloys, designated FAP, FA129, FA180 and FAL, were investigated. The nominal alloy compositions are given in Table 1.

Table 1. Alloy Composition (w/o)

Alloy	Cr	Al	Zr	Nb/Mo	C	B	S(ppm)
FAP	5.5	8.4	0.18	2.0 Mo	0.02		
FA129	5.5	15.8		1.0 Nb	0.05		
FA180	5.5	15.8	0.05	1.0 Nb, 1.6 Mo	0.10	0.01	
FAL	5.5	15.8	0.20			0.01	50

All the alloys contained 5.5 w/o Cr. As indicated, the main compositional differences were that FAP had a lower aluminum content (8.4 w/o) but contained 0.18 w/o zirconium; FA129, FA180, and FAL contained 15.8 w/o Al but had different zirconium levels (0 to 0.20 w/o) (Table 1). Therefore, comparison of FAP and FAL should provide insight into the role of aluminum content, while assessment of the oxidation behavior of FA129, FA180 and FAL should reveal the role of the zirconium level.

The specimens, typically 1 x 1 cm or 2 x 1 cm, were cut from sheets of these alloys having thicknesses between 0.23-0.70 mm. Each specimen was contained in an alumina crucible while being cyclically oxidized in either air or oxygen for successive periods ranging between 60 and 200 h (but usually 80 h) with intervening furnace cooling to room temperature. Total exposure times were about 1100 h. The oxidation temperature was 1300°C but, in addition,

FAP was oxidized at 1250°C. After each exposure period, the extents of attack and of oxide spallation were measured gravimetrically using analytical balances with accuracies of ± 0.05 mg (about ± 0.03 mg/cm^2). Before oxidation and after selected oxidation periods, the specimens were also photographed to provide information on dimensional changes caused by oxidation.

Following the completion of the exposures, the chemical and physical nature of the attack was characterized by a range of surface analytical procedures including x-ray diffraction (XRD), light microscopy, scanning electron microscopy (SEM), scanning transmission electron microscopy (STEM), energy dispersive x-ray analysis (EDAX) and electron microprobe analysis (EPMA).

RESULTS AND DISCUSSION

The oxidation behavior of these alloys was characterized by four main features: a protective regime, oxide spallation, oxidation-induced alloy dimensional growth, and breakaway attack. Increases in weight, expressed in terms of the original geometric surface area, with time for the individual FA129, FA180 and FAL specimens are shown in Fig. 1. Initially, the FAL oxidation kinetics were essentially parabolic, indicative of a protective oxidation regime, which x-ray diffraction and EPMA showed to have resulted from the formation of an αAl_2O_3 scale (Fig. 2). Up to ~50 h, the extents of attack of FA129, and also FA180, which also formed an $\alpha-Al_2O_3$ scale, were comparable to that of FAL, but thereafter they were progressively greater, as the oxidation kinetics of these alloys were effectively linear (Fig. 1).

Although oxide spalled from all the alloys on cooling to room temperature, there was a major difference between the behavior of FA129 and FA180 and that of FAL (Fig. 3). Scanning electron microscopy of both the planar and transverse scale sections of FA129 (Fig. 4) and of FA180 indicated that at room temperature these scales were buckled and friable. The scales almost completely spalled on every furnace cool, such that the weight of spalled oxide increased linearly with exposure time (Fig. 3). In contrast, although the scale on FAL contained defects (Fig. 2a), most of it remained adherent throughout oxidation and only a small fraction of the oxide spalled as discrete particles by a wedge type mechanism. Initially, failed scales appeared mainly adhesive but, on successive reoxidation and cooling became increasingly cohesive (Fig. 5). To highlight this difference in behavior of the two alloys, after 500 h of oxidation, the corresponding weights of spalled oxide were 26 mg/cm2 from FA129 and only 0.5 mg/cm2 for FAL.

As a result of oxidation, both the length and width of FAL specimens increased measurably (Fig. 6), although the values for the thinnest and most distorted FAL specimen are less certain because of the pronounced bending of this specimen caused by scale growth. Overall, the kinetics of area extension followed that of oxidation, in that it was fastest initially and continued at a rate which decreased progressively with time (Fig. 6). For 0.5 mm thick specimens the area had grown by ~35% prior to breakaway. Specimens of FA129 grew similarly as a result of oxidation, but by a smaller extent, with a 16% extension prior to breakaway.

At a critical cumulative weight gain, which increased with specimen thickness, the oxidation rates of FA129, FA180, and FAL abruptly accelerated as a result of the transformation from protective type oxidation to non-protective attack (Fig. 1). The time to the onset of breakaway lay between that of the last measurement in the protective regime and the first weighing following breakaway, which are the range of values shown in Fig. 7. As expected, the data in both air and oxygen at 1300°C were consistent. On exposure at this temperature, FAP, the alloy containing the lowest Al content, exhibited the worst behavior as it went immediately into non-protective oxidation. However, at 1250°C, breakaway followed an initial period of parabolic oxidation behavior.

Comparison of the data for the iron-aluminum alloys studied in oxidizing environments at 1300°C clearly indicated that both the zirconium and aluminum contents significantly affected their oxidation behavior. The role of zirconium was revealed by detailed characterization of the oxide scales formed on FA129 and FAL and by relating the oxide morphology to current understanding of the development and failure of protective alumina scales (for example, see ref. 3, 7-9). The alumina scale on FA129, which did not contain Zr, was similar to that formed on FeCrAl alloys[7] in that it was buckled, in the main being separated from the alloy with only localized areas of attachment (Fig. 4). In contrast, the corresponding scales on FAL containing 0.20 w/o Zr, were compact and mainly adherent (Fig. 2a). Electron microprobe anlaysis (Fig. 2b) indicated that the scale was enriched in zirconium, whose concentration was highest near the gas interface and decreased with scale depth. The Zr levels in the alloy became depleted and the concentrations shown in Fig. 4b are limits of measurement detection. Scanning electron microscopy an STEM with EDAX established that zirconium was present as discrete, 0.5-1.2 μm diameter ZrO_2 (monoclinic) particles (Fig. 8). Compositions of oxide grains at the protective scale surface shown in Fig. 8 are given in Table 2. Such segregation to the gas-scale interface has been observed for

several alumina-forming systems (see for example ref. 9). It would be expected,[9] and has now been observed experimentally,[10] that the zirconium was also segregated at oxide grain boundaries.

Table 2. EDAX Analysis of Particles A-I Shown in Fig. 8

Particle	Composition w/o			
	Al	Fe	Cr	Zr
A	84.6	14.6	0.8	--
B	93.0	7.0	--	--
C	92.8	6.0	--	1.2
D	47.3	2.8	--	49.1
E	91.6	5.9	--	2.6
F	88.7	8.0	0.2	3.1
G	4.7	2.9	--	92.4
H	38.6	41.5	2.3	17.6
I	2.4	3.5	0.1	94.0

The buckled alumina scale formed on FA129 at 1300°C could be assumed to have developed by the transport of both cations outwards and of oxidant inwards, with void formation at the metal-scale interface, rapid aluminum surface diffusion and possibly also aluminum vaporization. On cooling, this scale underwent tensile cracking and spalled readily.[11] On re-exposure of the alloy, scale regeneration was facilitated by the relatively high indigenous alloy aluminum content until this fell below the critical Al level for onset of breakaway. The linear oxidation kinetics were consistent with successive scale thickening and breakdown.

In its role as a reactive alloying addition, zirconium is known to improve the protection afforded by alumina scales[6,12] and appears to have acted in this manner in FAL, particularly in reducing both the initial mechanical and subsequent chemical failure of the scales. As a result of the segregation of zirconium to the oxide grain boundaries, outward cation transport would be inhibited such that the scale on FAL would have developed primarily by inward anion transport.[8-10] Although the oxide grains in the inner scale region were columnar (Fig. 5d), and thus consistent with inward growth, in the outer region they appeared to be equiaxed (Fig. 5a-c), which is associated with outward movement. This indicates that scale formation on FAL involved both transport mechanisms, possibly sequentially rather than, at least initially, coincidentally. The scales also contained defects (Fig. 2a), the size and extent of which increased with exposure time, which have been shown to play a significant role in instigating decohesion of alumina scales formed on the Y_2O_3-bearing FeCrAl ODS alloys.[13] However, the extent of spalling from FAL was smaller due presumably to the relief of stresses (resulting both from oxide growth at temperature and from the mismatch of the scale and alloy thermal expansion coefficients on furnace cooling) by deformation of the alloy

(Fig. 6). Like most wrought ferritic alloys, FAL has a low creep strength at ultrahigh temperatures.[4] As a consequence, the resultant compressive strain on the alumina scale responsible for wedge type mechanical failure[11] could be considerably lower than would have been experienced by a comparable scale on the stronger ODS alloys and which, in certain circumstances, caused scale spallation.[1, 3, 12] Since the mechanical properties of FA129 and FAL were comparable, the smaller extent of deformation of the former alloy during oxidation was attributable entirely to the respective scale morphologies. Finally, it should be noted that whereas a zirconium concentration of 0.2 w/o in the Fe_3Al type alloys proved to be effective, a factor of four lower level (0.05 w/o) was not.

With respect to the influence of aluminum concentration, there is a synergistic interaction between chromium and aluminum in the ability of FeCrAl alloys to form protective alumina scales. In the present series of iron-aluminum alloys, the chromium content was limited to 5.5 w/o. At this chromium level even a concentration of 8 w/o aluminum was insufficient for protective alumina scale formation at 1300°C, as shown by FAP, although it did contain 0.2 w/o zirconium. However, a protective type oxidation regime was established on this alloy at 1250°C and below. At 1300°C, the higher aluminum content (15.8 w/o) of the Fe_3Al alloys proved to be essential to assure protective scale formation.

The overall mechanism leading to breakaway oxidation of these alloys bears many similarities to that already modeled for the alumina forming FeCrAl+Y_2O_3 ODS alloys.[1-3] Non-protective oxidation (Fig. 9) occurred when the alloy aluminum content was reduced, by scale formation and spallation, to a value below that needed to sustain continuing growth of a protective, adherent, alumina scale. At this juncture rapid internal alumina formation was instigated at widely separated locations, which facilitated further depletion of the alloy Al content, such that the material behaved as a low alloyed ferritic steel. Non-protective oxidation ensued thus leading to the complete oxidation of the metal section with the formation of essentially iron oxides. The main features of the chemical sequence were apparent within the transition zone between the regions of protective and non-protective oxidation (Figs. 9 and 10). When the alloy aluminum content in the sub-scale region fell below the critical value, leading to internal oxidation, the associated stresses generated also caused mechanical failure of the alumina scale. This was then exacerbated by the subsequent rapid outward diffusion of iron leading to the formation of iron-rich oxide crystallites (Fig. 10) through what had been the protective alumina layer, which, in turn, became engulfed by this outward growing oxide layer (Fig. 9).

As mentioned already, the time to breakaway was dependent on several critical parameters. These included the extent of aluminum available (that is, the alloy aluminum content and specimen section thickness); the rate of aluminum consumption through oxidation, which would be enhanced by spallation; and the rate of aluminum diffusion from within the alloy to the oxidizing surface. As observed with the ODS FeCrAl-Y_2O_3 alloys,[3] aluminum diffusion was rapid, as EPMA (Fig. 2b) indicated no perceptible aluminum concentration gradient across FAL. A final parameter is the concentration of the residual alloy aluminum content prior to breakaway attack. This could be calculated from the last weight gain prior to breakaway and also measured on metallographic cross sections by EPMA of the alloy beneath protective oxide scales adjoining regions which had oxidized completely following breakaway (although these latter values could be on the low side). For FAL, the calculated values ranged between 3.1-5.8 w/o, while the EPMA values were between 1.8 and 2.4 w/o. These were slightly higher than the corresponding calculated residual Al contents of the ODS alloys[1-3] for which the average of fifteen values, ranging between 0.3 and 3.5 w/o, was 1.8 w/o. For FA129, the calculated and EPMA residual critical aluminum content values, 4.0-7.2 w/o and 4.9 w/o, respectively, were higher than those for FAL.

The measured times to breakaway for the three Fe_3Al alloys are compared in Fig. 7 with the corresponding data for the Y_2O_3-bearing FeCrAl ODS alloys.[1-3] The FAL data fell on or lay slightly above the best estimate line through the ODS results. This was probably entirely coincidental but does demonstrate that the behavior of this Fe_3Al alloy is at least as good as the best ferritic alloys that are currently commercially available (see ref. 14 also). Additionally, this observation suggests that the potential offered by the higher aluminum content of FAL was not being fully exploited. The two reasons for the lower than expected performance of FAL compared with the ODS FeCrAl alloys are (1) the slightly higher residual aluminum alloy content for breakaway and, more significantly, (2) the higher oxidation rate of FAL. An Arrhenius plot of available isothermal and cyclic data for aluminum consumption through oxidation is shown in Fig. 11, which indicates that at 1300°C the FAL parabolic rate constant (40×10^{-2} mg cm^{-4} h^{-1}) was over an order of magnitude higher than that for the ODS alloy, ODM 751 (2.5×10^{-2} mg^2 cm^{-4} h^{-1}). Although the causes of this disparity are not known, two important factors undoubtedly are differences in the high-temperature mechanical properties and the chemical role of the minor alloy additions, especially reactive elements, in the respective alloy types.

CONCLUSIONS

1. The oxidation behavior of iron-aluminum alloys in oxidizing environments at 1300°C was improved by an aluminum content of at least 15.8 w/o and by the addition of zirconium, with 0.2 w/o being more effective than 0.05 w/o. This reduced the oxidation rate and the propensity for the subsequent mechanical and chemical failure of the alumina scale formed.

2. For the iron aluminides, the time to onset of non-protective oxidation was controlled by the available Al reservoir, the rate of Al consumption through oxidation and the critical residual alloy Al content needed to sustain alumina scale integrity.

3. Times to the onset of breakaway were similar for Fe_3Al-Zr and commercial FeCrAl alloys containing Y_2O_3 (such as MA 956, PM 2000 and ODM751) because the lower aluminum consumption rate of the latter alloys offset the benefits of the higher initial aluminum content of Fe_3Al-Zr.

Acknowledgments

The authors acknowledge J. A. Horton for the STEM analysis and M. Howell for experimental support. They thank J. R. DiStefano, B. A. Pint, and I. G. Wright for their reviews of the manuscript. This research was sponsored by the Fossil Energy Advanced Research and Technology Development (AR&TD) Materials Program, U.S. Department of Energy, under contract DE-AC05-96OR22464 with Lockheed Martin Energy Research Corporation.

References

1. M. J. BENNETT, R. PERKINS, J. B. PRICE, and F. STARR: 'The Oxidation Behavior of Alumina Forming Ferrite Oxide Dispersion Strengthened Alloys,' *Materials for Advanced Power Engineering*, D. Cousouradis, et al., ed., Kluwer Academic Publishers 1994, **2**, 1553-1562.

2. W. J. QUADAKKERS and M. J. BENNETT, 'Oxidation Induced Lifetime Limits of Thin Walled Iron Based Alumina Forming Oxide Dispersion Strengthened Alloy Components,' *Mater. Sci. and Tech.*, 1994, **10**, 126-131.

3. M. J. BENNETT, 'Recent Studies and Current Problems Concerning the High Temperature Oxidation Behavior of Alumina Forming Iron Based Alloys,' *Solid State Phenomena*, 1995, **41**, 235-252.

4. C. G. MCKAMEY, J. H. DEVAN, P. F. TORTORELLI, and V. K. SIKKA, 'A Review of Recent Developments in Fe_3Al Based Alloys,' *J. Mater. Res.*, 1991, **6**, 1779-1805.

5. J. H. DEVAN and P. F. TORTORELLI, 'The Oxidation-Sulphidation Behavior of Iron Alloys Containing 16-40% av. % Aluminium,' *Corros. Sci.*, 1993, **35**, 1065-1071.

6. P. F. TORTORELLI and J. H. DEVAN, 'Compositional Influences on the High-Temperature Corrosion Resistance of Iron Aluminides,' pp. 257-70 in Processing, Properties, and Applications of Iron Aluminides, J. H. Schneibel and M. A. Crimp, eds., The Minerals, Metals, and Materials Society, Warrendale, PA, 1994.

7. F. A. GOLIGHTLY, F. H. STOTT, and G. C. WOOD, 'The Influence of Yttrium Additions on the Oxide-Scale Adhesion on Fe-Cr-Al Alloys,' *Oxid. Met.*, 1976, **10**, 163-167.

8. R. PRESCOTT and M. J. GRAHAM, 'The Formation of Alumina Scales on High Temperature Alloys,' *Oxid. Met.*, 1992, **38**, 233-255.

9. B. A. PINT, 'Experimental Observations in Support of the Dynamic-Segregation Theory to Explain the Reactive Element Effect,' *Oxid. Met.*, 1996, **45**, 1-37.

10. K. B. ALEXANDER, K. PRUSSNER, P. Y. HOU, and P. F. TORTORELLI, 'Microstructure of Alumina Scales and Coatings on Zr-Containing Iron-Aluminide Alloys,' These Proceedings.

11. H. E. EVANS, 'Modeling Oxide Spallation,' *Matl.at High Temp.*, 1994, **12**, 219–227.

12. C. S. BARRETT, *Oxid. Met.*, **30** (1988), 337-355.

13. J. P. WILBER, M. J. BENNETT, and J. R. NICHOLLS, 'Evaluation of the Composite Defect Size in Alumina Scales Formed on ODS Alloys,' 1996, These Proceedings.

14. I. G. WRIGHT, B. A. PINT, C. P. SIMPSON, and P. F. TORTORELLI, High-Temperature Oxidation Life Characteristics of ODS-Fe_3Al,' accepted for publication in Mater. Sci. Forum, 1996.

Figure Captions

Fig. 1. Comparison between the cyclic oxidation kinetics of FA129, FA180, and FAL in air at 1300°C.

Fig. 2. Scanning electron micrograph [A] and EPMA line traces [B] across a transverse section of the alumina scale formed on FAL following 350 h of oxidation in air at 1300°C.

Fig. 3. Comparison between the extents of cumulative oxide spallation following the discontinuous oxidation of FA129, FA180, and FAL in air at 1300°C with intermediate cooling to room temperature. The specimen thicknesses are denoted by the same symbols described in Fig. 1.

Fig. 4. Scanning electron micrograph of a transverse section of alumina scale formed on FA129 following 80 h oxidation in air at 1300°C.

Fig. 5. Scanning electron micrographs of the protective scale on FAL after 1101 h of oxidation at 1300°C showing [A] where oxide had spalled, [B] the scale outermost surface, [C] the spall section edge, and [D] the base of the spall region.

Fig. 6. Comparison between the percentage increase in area of FAL and FA129 with duration of oxidation in air at 1300°C. The specimen thicknesses are denoted by the same symbols described in Fig. 1.

Fig. 7. Influence of alloy thickness on the time to breakaway oxidation of FAP, FA129, and FAL in air and oxygen at 1300°C and compared with the corresponding data for the ODS alloys MA 956, PM 2000 and ODM 751 (References 1-3).

Fig. 8. Scanning electron micrograph of the protective scale formed on FAL after 1101 h of oxidation in oxygen at 1300°C. EDAX analyses of particles A-I are given in Table 2.

Fig. 9. Electron image [A] of a FAL cross section after 1101 h of oxidation in oxygen at 1300°C together with the Fe, Al, and Cr x-ray images ([B]-[D]) of the area shown in [A]. In [A] P denotes the protective scale, T the transition zone, and B breakaway attack.

Fig. 10. Scanning electron micrographs of FAL after 350 h oxidation in air at 1300°C showing the topography of [A] the protective scale and transition zone, [B] the breakaway attack, [C] and [D] the transition zone.

Fig. 11. Arrhenius plots comparing the parabolic rate constants for the aluminum consumption by oxidation of FAL, FeAl, Fecralloy steel, ODM 751 and NiAl at 800-1300°C.

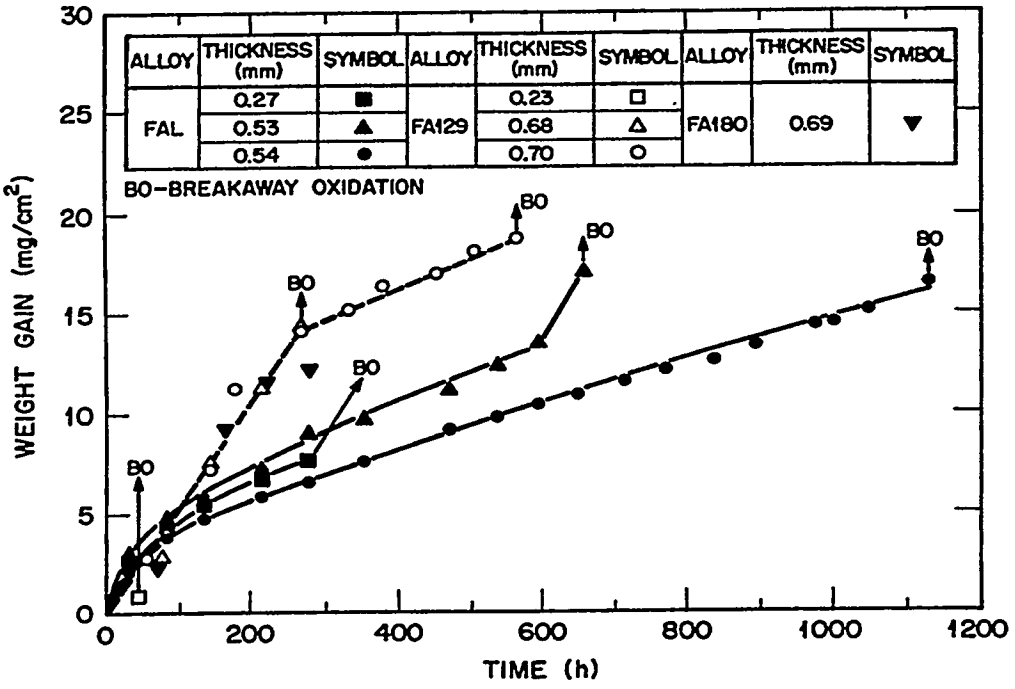
ALLOY
THICKNESS (mm)
SYMBOL
FAL
0.27
0.53
0.54
FA129
0.23
0.68
0.70
FA180
0.69
BO-BREAKAWAY OXIDATION
BO
WEIGHT GAIN (mg/cm²)
TIME (h)
0
5
10
15
20
25
30
200
400
600
800
1000
1200

Fig. 1.

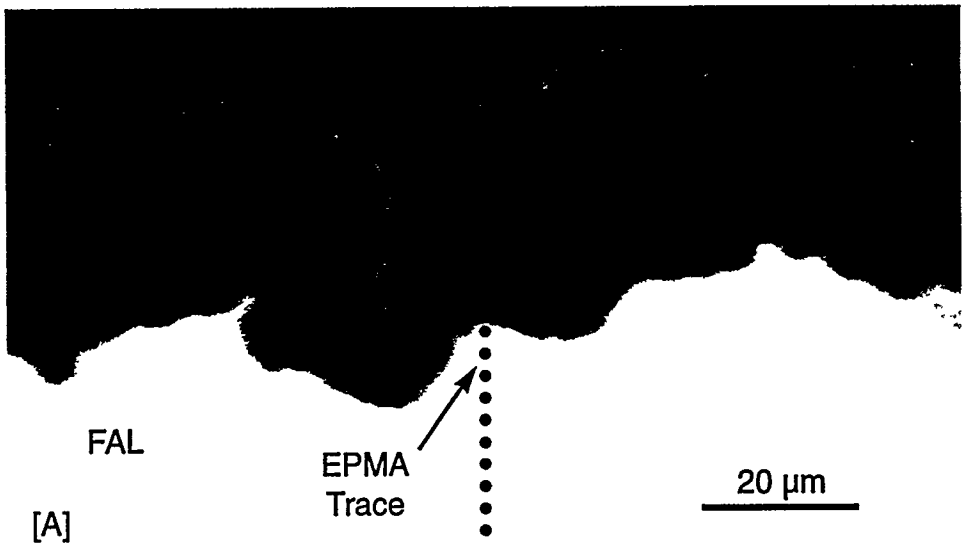
FAL
EPMA
Trace
20 µm
[A]

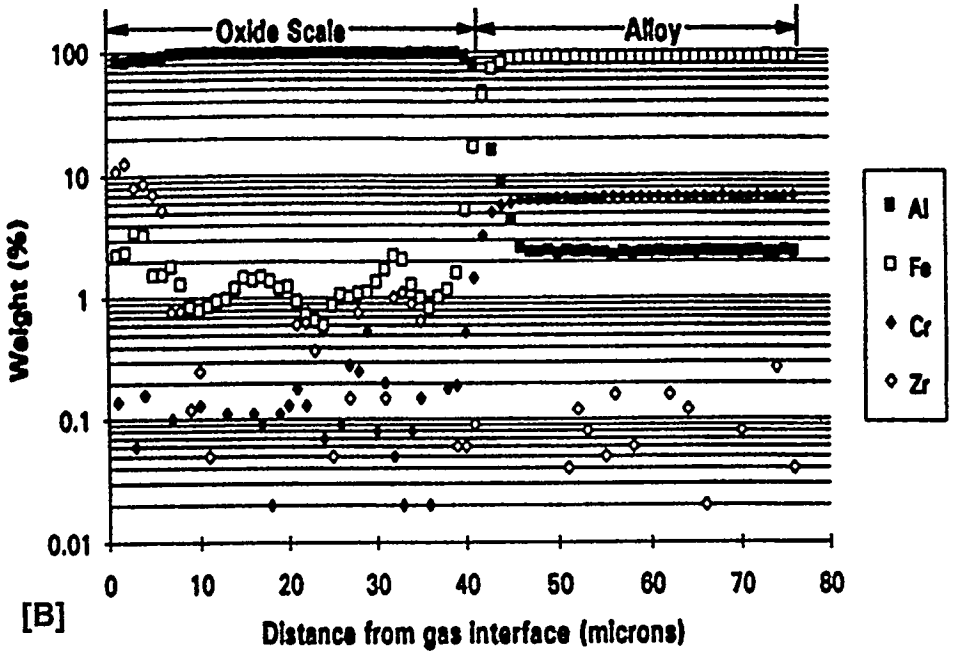
Oxide Scale
Alloy
100
10
1
0.1
0.01
Weight (%)
0
10
20
30
40
50
60
70
80
Distance from gas interface (microns)
Al
Fe
Cr
Zr
[B]

Fig. 2

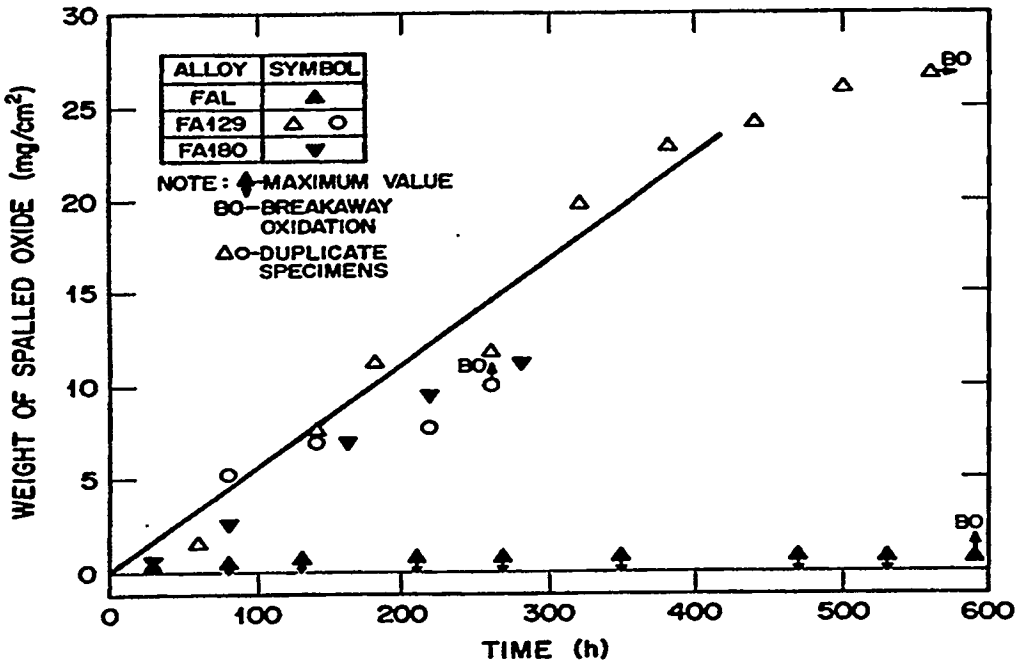
WEIGHT OF SPALLED OXIDE (mg/cm²)
TIME (h)
ALLOY
SYMBOL
FAL
FA129
FA180
NOTE: ↕ MAXIMUM VALUE
BO—BREAKAWAY OXIDATION
Δo—DUPLICATE SPECIMENS
BO
BO
BO
0
5
10
15
20
25
30
0
100
200
300
400
500
600

Fig. 3.

Fig. 4

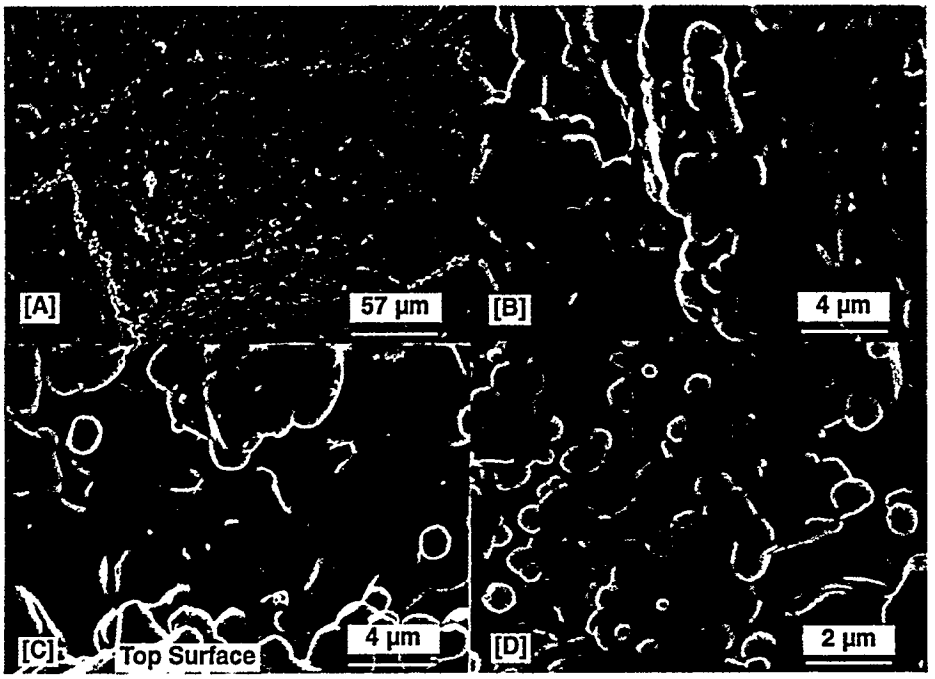

Fig. 5

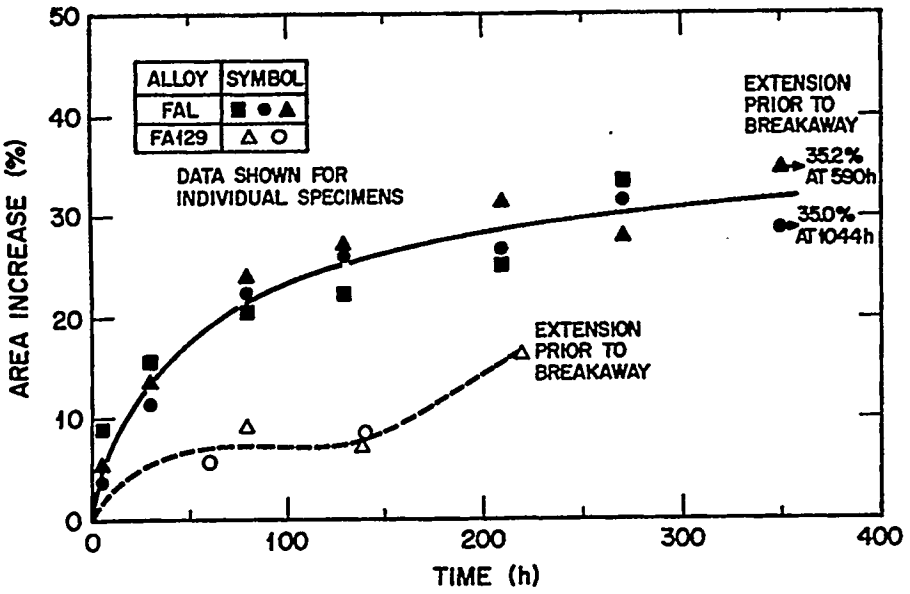
ALLOY
SYMBOL
FAL
FA129
DATA SHOWN FOR INDIVIDUAL SPECIMENS
EXTENSION PRIOR TO BREAKAWAY
35.2% AT 590h
35.0% AT 1044h
EXTENSION PRIOR TO BREAKAWAY
AREA INCREASE (%)
TIME (h)
0
10
20
30
40
50
0
100
200
300
400

Fig. 6

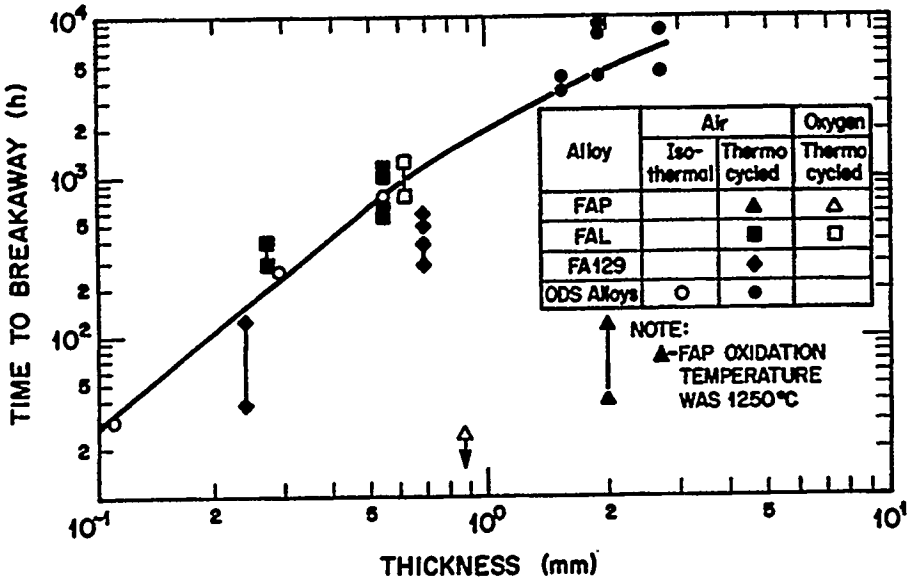
TIME TO BREAKAWAY (h)
THICKNESS (mm)
Alloy
Air
Oxygen
Iso-thermal
Thermo cycled
Thermo cycled
FAP
FAL
FA129
ODS Alloys
NOTE:
▲-FAP OXIDATION TEMPERATURE WAS 1250°C

Fig. 7

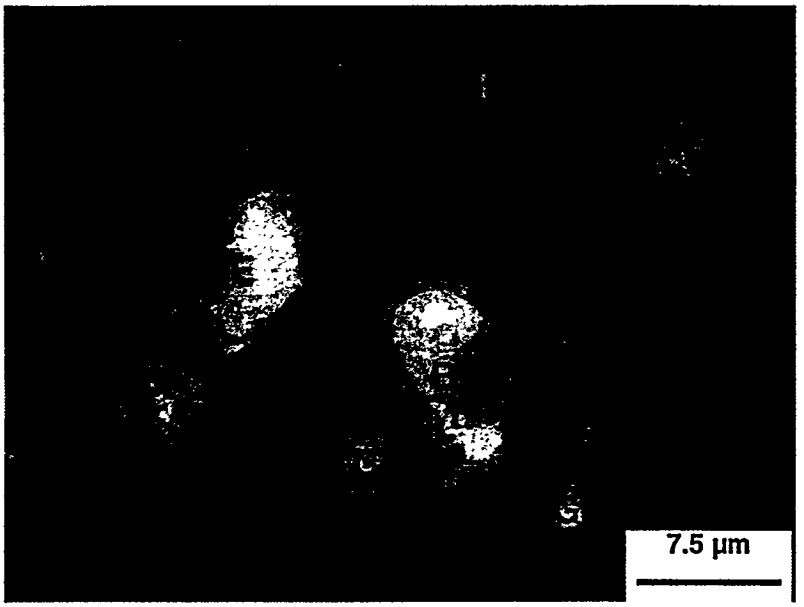

Fig. 8

Fig. 9

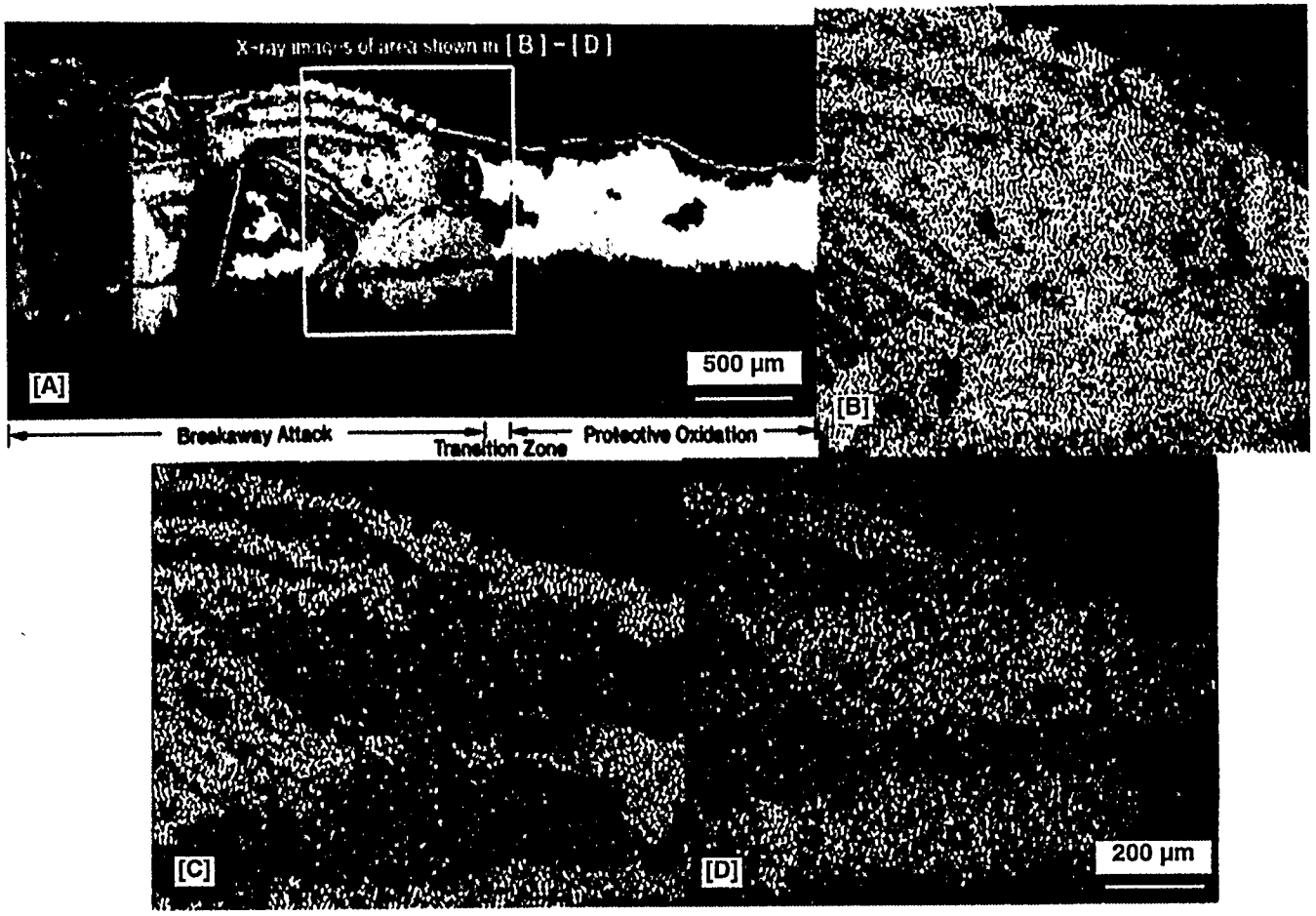
X-ray images of area shown in [B] - [D]
500 µm
[A]
Breakaway Attack
Transition Zone
Protective Oxidation
[B]
[C]
[D]
200 µm

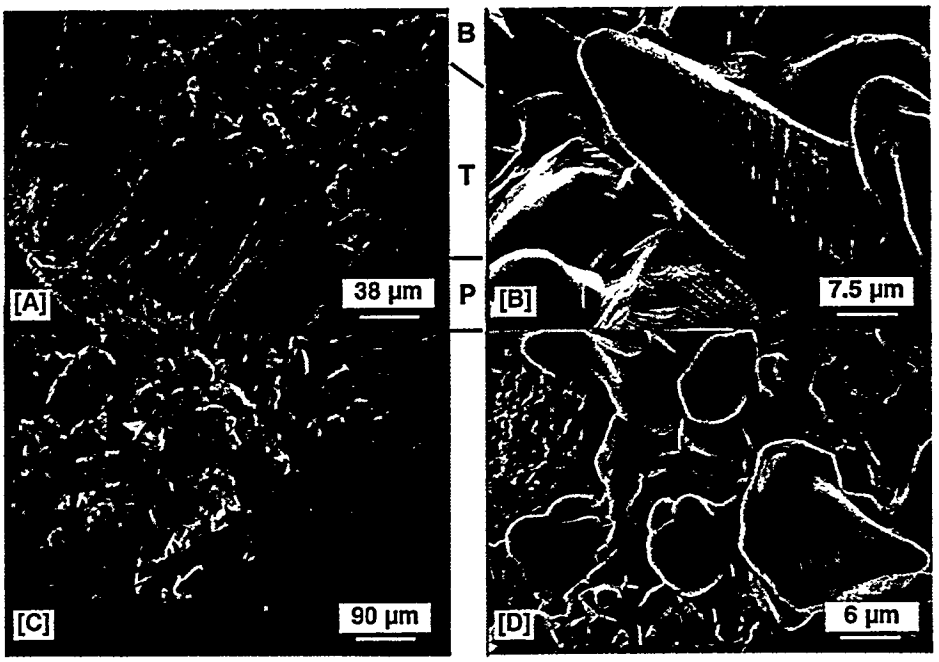

Fig. 10

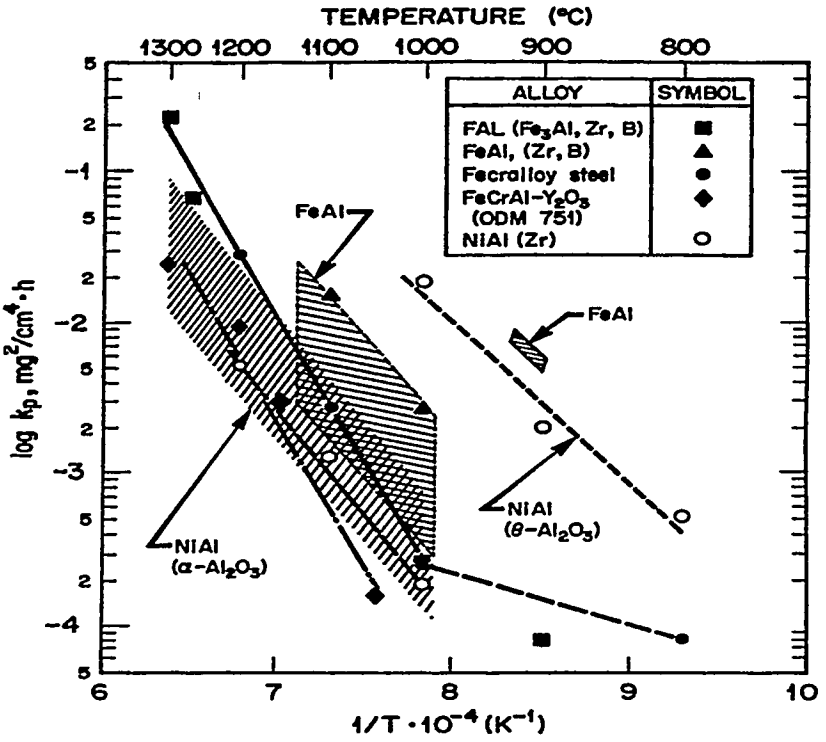
TEMPERATURE (°C)
1300 1200 1100 1000 900 800
ALLOY
SYMBOL
FAL (Fe_3Al, Zr, B)
FeAl, (Zr, B)
Fecralloy steel
FeCrAl-Y_2O_3 (ODM 751)
NiAl (Zr)
FeAl
FeAl
NiAl (α-Al_2O_3)
NiAl (θ-Al_2O_3)
log k_p, $mg^2/cm^4 \cdot h$
$1/T \cdot 10^{-4}$ (K^{-1})
6
7
8
9
10

Fig. 11